Received: 20 October 2020 | Revised: 15 December 2020 | Accepted: 31 December 2020

DOI: 10.1111/cas.14795

ORIGINAL ARTICLE

Cancer Science WILEY

Single-cell transcriptome analysis revealed the heterogeneity and microenvironment of gastrointestinal stromal tumors

Xiaofan Mao[1,2] | Xuezhu Yang[3] | Xiangping Chen[1,2] | Sifei Yu[1,2] | Si Yu[3] | Beiying Zhang[1,2] | Yong Ji[3] | Yihao Chen[1,2] | Ying Ouyang[1,2] | Wei Luo[1,2]

[1]Clinical Research Institute, The First People's Hospital of Foshan & Sun Yat-Sen University Foshan Hospital, Foshan, China

[2]Medical Engineering Technology Research and Development Center of Immune Repertoire in Foshan, The First People's Hospital of Foshan & Sun Yat-Sen University Foshan Hospital, Foshan, China

[3]Gastroenterology, The First People's Hospital of Foshan & Sun Yat-Sen University Foshan Hospital, Foshan, China

Correspondence
Wei Luo, Clinical Research Institute, Foshan Hospital, Sun Yat-sen University, Foshan 528000, Guangdong, China.
Email: luowei_421@163.com

Funding information
Medical Engineering Technology Research and Development Center of Immune Repertoire in Foshan, Foshan City Climbing Peak Plan (Grant/Award Number: 2019A004, 2019D035, 2019D036), Science and Technology Innovation Platform in Foshan City (Grant/Award Number: FS0AA-KJ218-1301-0007), Foundation and Applied Basic Research Fund of Guangdong Province (Grant/Award Number: 2019A1515110676, 2019A1515110677), National Natural Science Foundation of China (Grant/Award Number: 81972335).

Abstract

Gastrointestinal stromal tumor (GIST) is the most common mesenchymal tumor of the human gastrointestinal tract. In this study, we performed single-cell RNA sequencing (RNA-seq) on intra- and peri-tumor tissues from GIST patients with the aim of discovering the heterogeneity of tumor cells in GIST and their interactions with other cells. We found four predominating cell types in GIST tumor tissue, including T cells, macrophages, tumor cells, and NK cells. Tumor cells could be clustered into two groups: one was highly proliferating and associated with high risk of metastasis, the other seemed "resting" and associated with low risk. Their clinical relevance and prognostic values were confirmed by RNA-seq of 65 GIST samples. T cells were the largest cell type in our single-cell data. Two groups of $CD8^+$ effector memory (EM) cells were in the highest clonal expansion and performed the highest cytotoxicity but were also the most exhausted among all T cells. A group of macrophages were found polarized to possess both M1 and M2 signatures, and increased along with tumor progression. Cell-to-cell interaction analysis revealed that adipose endothelial cells had high interactions with tumor cells to facilitate their progression. Macrophages were at the center of the tumor microenvironment, recruiting immune cells to the tumor site and having most interactions with both tumor and nontumor cells. In conclusion, we obtained an overview of the GIST microenvironment and revealed the heterogeneity of each cell type and their relevance to risk classifications, which provided a novel theoretical basis for learning and curing GISTs.

KEYWORDS

cell interactions, gastrointestinal stromal tumor, metastasis-associated genes, single-cell sequencing, tumor heterogeneity

Mao, Yang and Chen equally contributed to this study.

1 | INTRODUCTION

Gastrointestinal stromal tumor (GIST) is the most common mesenchymal tumor of the human gastrointestinal (GI) tract, with an incidence rate of 1.5 per 100 000 people per year.[1] It is mostly found in the stomach (60%) or small intestine (25%),[2] accounting for 80% of all GI mesenchymal neoplasms and 0.1%-3% of all gastrointestinal malignancies.[3] In the 1980s, GIST was described as a type of smooth muscle tumor. However, with the development of pathology and immunohistochemistry, GIST has been proved to be a completely separated entity and has its own clinicopathologic characteristics, histogenesis, and differential diagnosis.[4]

It is widely accepted that GISTs arise from the lineage of interstitial cells of Cajal (ICC),[5] a class of fibroblast-like interstitial cells[6] sharing many molecular biomarkers, such as *KIT* (CD117), a receptor tyrosine kinase. GISTs are most commonly (over 85%) caused by mutually exclusive gene mutations on *KIT* or *PDGFRA*, which controls the tyrosine kinase receptors and causes constitutional activation, leading to neoplastic growth of cells from the ICC lineages.[5,7] GISTs without mutations from *KIT* and *PDGFRA* are known as wild type. Based on cytomorphology, GISTs can be divided into three types: spindled (70%), epithelioid (20%), and mixed (10%). The spindle cell type highly expresses *KIT*, making it not difficult to diagnose, while the epithelioid type shows different *KIT* staining in different genetic backgrounds.[8] Overall, *KIT* expression is present in over 90% of cases, *PDGFRA* in 80%, *DOG-1* in 98%, and *CD34* in 80%.

About 30% of GISTs are malignant. Based on tumor size, tumor site, and mitotic count, the risk stratification system classifies GISTs into four categories: very low, low, intermediate and high risk.[9,10] This classification system provides reliable risk assessments and is applied by the Armed Forces Institute of Pathology (AFIP) criteria and the National Comprehensive Cancer Network (NCCN) risk criteria.[11] For localized and resectable GISTs larger than 2 cm, the main treatment remains surgical resection. High-risk patients with mutations sensitive to imatinib, a tyrosine kinase inhibitor, should be treated with imatinib for 3 years or until drug resistance occurs.

Understanding of GISTs is expanding rapidly in multiple areas of epidemiology, pathophysiology, histopathology, diagnosis, treatments, and prognosis. However, we still do not clearly know the etiology of GISTs and the heterogeneity within tumor cells, and how other cells act in GIST microenvironment. In particular, the interactions of GI tumor cell heterogeneities with distinct lymphocytes are unknown. More studies need to be carried out on the particular profiles and functions of tumor associated macrophages (TAMs) and T cells, and other lymphocyte subtypes, including natural killer (NK) cells, B cells, etc. Investigating these points could help us to better understand GIST microenvironments and find potential targets for diagnose, prognosis, and therapy. We therefore performed single-cell transcriptome analysis of GIST tumor tissues resected from two patients of low and high risk in an attempt to discover the heterogeneity of GISTs and their interactions with the immune cells as well as other cell types.

2 | MATERIALS AND METHODS

2.1 | Sample collection and clinical information

Two patients (G1 and G2) were recruited in our study. Patient G1 (male, age 68) underwent laparoscopic mass resection surgery shortly after his diagnosis. The size of tumor from patient G1 was about 5 × 4 × 3.5 cm. The tumor did not invade the gastric mucosa and the surrounding cautery edge was clean. The risk stratification for patient G1 was low risk. The mitotic index was 4/50 high power field (HPF). The immunohistochemical results were CD117(+), DOG-1(+), CD34(+), SMA(−), Desmin(−), h-CD(+), S-100(−), and Ki-67(5%+).

Patient G2 (male, age 62) was a high-risk patient. When patient G2 was diagnosed as GIST, the immunohistochemical results were CD117(+), DOG-1(+), CD34(+), SMA(−), S-100(−), and Ki-67(10%+). The tumor size was 6.7 × 5.2 × 5.8 cm, estimated by computed tomography. Multiple round slightly low-density lesions were seen in the liver. Proliferative lymph nodes were observed around the stomach, hepatic portal, and retroperitoneum. After 4 months of imatinib therapy, the tumor size decreased to 5.8 × 5.5 × 4.5 cm, and the liver lesions disappeared. The mitotic index was 6/50 HPF. At this time, laparoscopic mass resection surgery was implicated. The immunohistochemical results after surgery were CD117(+), DOG-1(+), CD34(+), CK(−), SMA(−), Desmin(−), S-100(−), and Ki-67 (15%+).

From both patients we collected intra-tumor and peri-tumor tissues of the same amount about 1 × 1 × 2 cm from the center and the edge of tumors, respectively.

2.2 | Single-cell suspension preparation and single-cell RNA library construction

Tumor tissues, obtained from laparoscopic mass resection surgery, were immediately sent to undergo the process of single-cell suspension preparation. Tissues were cut into small pieces and digested in incomplete Roswell Park Memorial Institute 1640 with endotoxin-free collagenasel (2 mg/mL; Sigma-Aldrich) for 1 hour at 37°C. The digested fragments were filtered through a 100-μm cell nylon mesh (BD Bioscience PharMingen) and washed twice in Hanks' balanced salt solution. Five milliliters of erythrocyte lysis solution was added to the cell suspension for 5 minutes and then phosphate buffer saline was added to stop the reaction and the product was washed twice.

Single-cell 5′ RNA and T cell VDJ libraries were generated by restrictedly following the user guide of Chromium Single Cell V(D)J Reagent Kits (CG000086 Rev J) in 10X genomics.

2.3 | Sequencing and quality control

We used Illumina Hi-seq X10 150PE for sequencing. Sequencing depth was set as suggested by 10X genomics. Using Cellranger 3.0 (10X genomics provided) software we generated cells × genes matrixes with all parameters set to default.

2.4 | Transcriptome data analysis

Cells were removed if they satisfied the following conditions: (a) RNA counts were less than 600; (b) RNA counts were larger than 98% of cells; and (c) mitochondrial gene expression percentages were more than 15%.

Data integration could be separated into two steps. In the first step, we used the "aggr" function in Cellranger3.0 to integrate data from the same batch. In the second step, we applied the SCTransform normalization method[12] using 5000 genes as high variable gene set and integrated data from different batches by Seurat.[13]

Thirty principal components were selected for cell clustering and UMAP visualization. Resolution was set to 1.5. Cells were aligned to BLUEPRINT[14] and ENCODE[15] using SingleR package.[16] Based on the alignments and well-known cell markers, clusters were assigned to the corresponding cell groups. We then retrieved cell members from each cell group to perform subgroup analysis. Normalization and data integration were re-run for each cell group. If a subgroup highly expressed the marker genes which should uniquely expressed on other cell groups, we considered it to be a mixed cell type generated by doublets. Such subgroups were removed.

Pseudo-time analysis was conducted to reveal the development of cell groups using the Diffusion Map algorithm[17] (destiny package in R). Directions of cell development were estimated by Velocity.[18]

2.5 | Gene set enrichment analysis (GSEA) and gene expression score calculation

Gene sets were obtained from MSigDB[19] including the gene sets from REACTOME,[20] KEGG,[21] and ImmuneSigDB.[22] Gene set enrichment analysis between two cell groups was performed by GSEA.[19] Pathway networks were visualized by Cytoscape.[23] For customized gene set comparisons among multiple cell groups, we calculated the scores of gene sets using the AUCell package in R. This method was also applied in bulk RNA-seq data to calculate corresponding scores.

Single gene expression score calculation was also based on the gene set constructed by the top 30 correlated genes, including the target gene itself. The AUCell package was used to calculate the scores.

2.6 | Calculation of macrophage polarization scores

Raw count matrixes of macrophage data were obtained from Gene Expression Omnibus (GEO) (GSE135165[24] and GSE117970[25]) as reference data. Using SingleR,[16] we aligned the RNA counts of single-cell transcriptome to the reference data and obtained the automatic annotation labels and polarization scores for each label. This method was also applied to calculate similarities among tumor cells, GIST cell line and cancer-associated fibroblast (CAF) using GSE143547 as reference.

2.7 | Weighted gene co-expression network analysis on tumor cells

Weighted gene co-expression network analysis (WGCNA)[26] was performed on tumor cells to retrieve coexpression gene models using the WGCNA package in R. The scores for each model were also obtained from this analysis. Receiver operating characteristic (ROC) analysis was performed between two groups of tumor cells based on the scores of the gene model using the pROC package in R.

2.8 | Calculation of clonotype Morisita-Horn similarities between two T cell subgroups

Morisita-Horn (MH) similarities[27] were used to estimate the clonotype similarities between two αβ T cell subgroups. The calculation was based on the formula:

$$\text{MH similarity} = \frac{2\sum_{i=1}^{S} x_i y_i}{\left(\frac{\sum_{i=1}^{S} x_i^2}{X^2} + \frac{\sum_{i=1}^{S} y_i^2}{Y^2}\right) XY}$$

where x is the number of cells with the shared clonotype in the total X cells from one group, y is the number of cells with the shared clonotype is presented in the total Y cells from the other group, and S is the number of unique shared clonotypes in the two cell groups.

2.9 | Interaction network construction

To investigate cell group-to-group interactions we applied the CellPhoneDB method[28] with built-in curated databases of cell surface molecule interactions. Interaction counts were calculated based on the "SCT" count matrix generated by Seurat from total cells in patients G1 and G2. Cell chemokine interactions were analyzed by retrieving chemokine interactions from the built-in databases in CellPhoneDB.

2.10 | Bulk RNA profiling of tumor tissues from GIST patients

Gene expression matrices of tumor tissues from GIST patients were downloaded from GEO. Two cohorts were collected. Cohort one comprised RNA-seq data from 65 primary and metastasis samples with AFIP risk classifications (GSE136755[29]). Cohort two contained RNA profiling by array from three primary gastric GISTs without synchronous or metachronous metastasis and five metastatic liver tumors originated from gastric GIST (GSE21315).

2.11 | Immunohistochemistry assay

Intra- and peri-tumor issues from a low-risk patient were used in immunohistochemistry assay. The formaldehyde fixed-paraffin embedded FFPE samples were sliced into 4-μm thick sections for histological and immunohistochemistry staining. The inflammatory cell infiltration level was examined by using hematoxylin and eosin (HE) staining. CD3, CD4, CD8, CD19, CD68, CD56, and CD117 were stained to reveal corresponding cell locations.

2.12 | Method of statistical analysis

A one-way ANOVA test was used to determine the statistical significance of data with multilevels followed by Turkey multiple comparisons. The Wilcoxon signed-rank test was used to determine the statistical significance of data with two levels. *P* values of .05 or less were considered statistically significant. Statistical calculations were performed with R.

3 | RESULTS

3.1 | Single-cell transcriptome analysis identified cell compositions within tumor tissue

We have performed the 10X single-cell analysis on the four samples of the intra- and peri-tumor tissues from two patients with low and high risk, respectively (Figure 1A), and obtained 10 786 and 19 977 effective cells in patients G1 and G2, respectively. Single cell RNA-seq

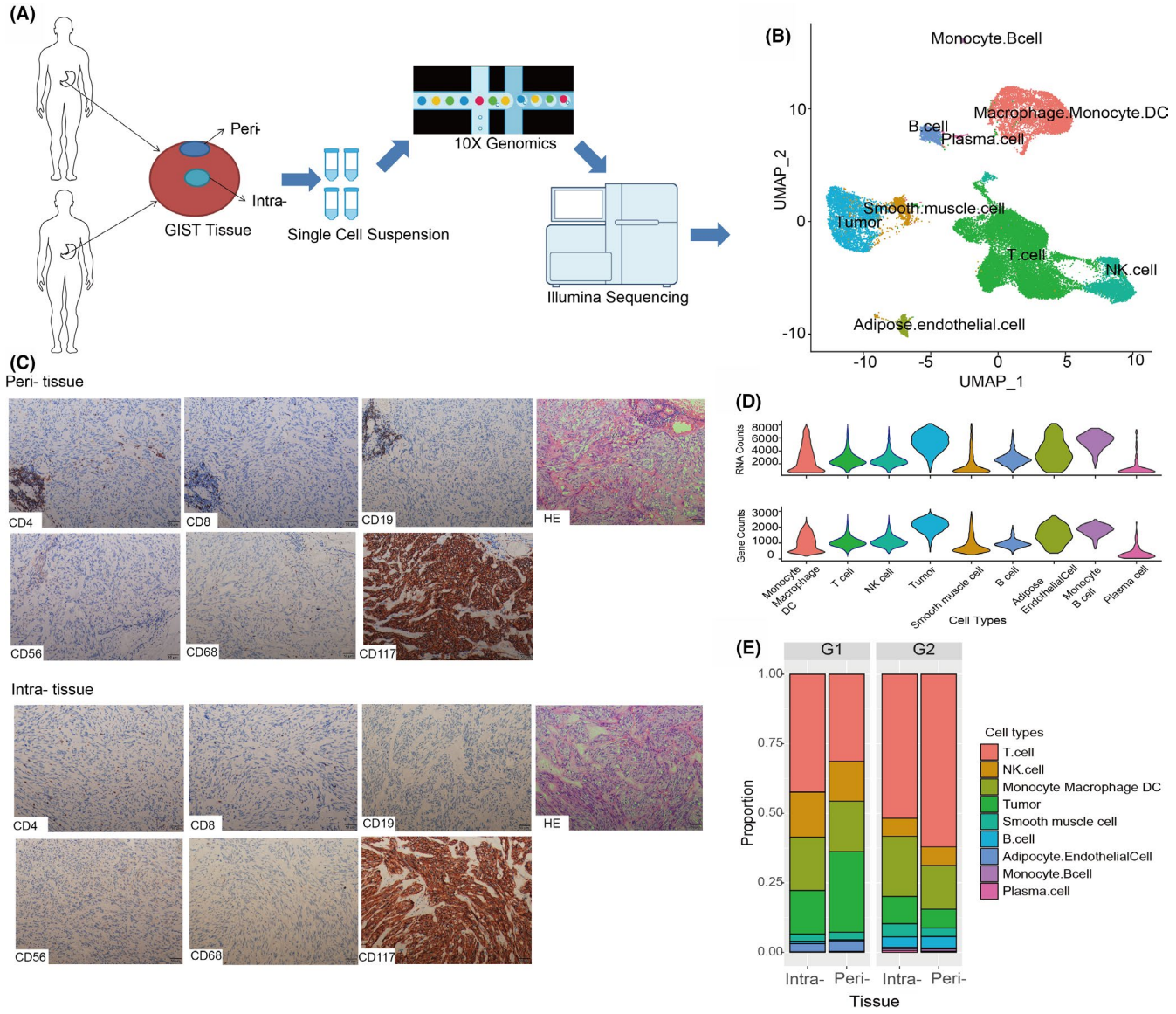

FIGURE 1 The cell type classifications in GIST tumor tissue. A, Single-cell sequencing flow chart. B, UMAP exhibits the cell type constructions in GIST. C, BLUEPRINT and ENCODE annotations on all cell clusters. Labels were automatically annotated by SingleR. D, The RNA and gene counts of all cell types. E, The barplot of the composition of all cell types in intra- and peri-tissue from patients G1 and G2

data can be downloaded on GEO with accession number GSE162115. We identified four major cell types in GIST tumor tissue, including tumor cells, monocytes/macrophages/dendritic cells (MMDs), T cells, and NK cells (Figure 1B). There were also other minor cell types such as B cells, smooth muscle cells, plasma cells, and adipose endothelial cells. Among all cell types, immune cells were the largest cell type we collected, accounting for 74.7% and 86.7% of total cells in patients G1 and G2, respectively. The immunohistochemistry of tumor samples revealed the localization of corresponding immune cells (Figure 1C). The representative staining showed that most lymphocytes and macrophages invaded in both peri- and intra-tissues.

Within our expectation, different cell types expressed different counts of RNA and gene, among which the tumor cells expressed the highest counts (Figure 1D). When investigating the cell type distributions across all four tissues, we did not find large changes between intra- and peri-tumor tissues (Figure 1E). Even in different patients, most cell types exhibited similar abundances. Collectively, our data exhibited four major cell types in GIST tissues, and the proportions of these cell clusters were mostly stable between tissues and individuals.

3.2 | Tumor cells in GIST exhibit high heterogeneities

Tumor cells heterogeneities in GISTs were not fully investigated in previous research. In our cases, tumor cell groups could be identified by commonly used biomarkers such as KIT, PDGFRA, DOG-1, and CD34 (Figure S1a-e). Notably, we found there were two major groups of tumor cells (Figure 2A), Tumor.C1 and Tumor.C2, which did not show great differences between patients or tissue types (Figure 2B). Both groups were similar to fibroblasts (Figure S2a). By further comparing these groups to the published transcriptome dataset (GSE143547) of the CAF and GIST cell line, we found over 97% cells were aligned in the GIST cell line 882 and T1 (Figure 2C), confirming that both groups of tumor cells were separated lineages from CAFs.

GIST biomarkers were generally expressed in both tumor cell groups (Figure S2b-e), reminding us that commonly used biomarkers are not able to elucidate tumor heterogeneities. By further analysis of gene differential expression tests (Figure 2D) and GSEA (Figure 2E) between the two tumor cell groups, we found that Tumor.C1 might be at a fast growing and late state of tumor development. First, the eukaryotic translation initiation factor gene, *EIF5*, was most significantly up-regulated in Tumor.C1, suggesting a high rate of protein synthesis. Second, a number of genes from heat shock protein families, such as *Hsp70*, *Hsp40*, *Hsp10*, and *Hsp60*, were also up-regulated in Tumor.C1, emphasizing the response of high stresses. Third, the TP53 pathway was observed to be enriched in Tumor.C1, indicating greater DNA damage compared to Tumor.C2. Furthermore, the enriched cell cycle and proliferation pathways in Tumor.C1 directly referred to a fast expanding status as high-grade malignancy in tumor development. In addition, Tumor.C1 expressed fewer human leukocyte antigen (HLA) molecules (Figure 2F), contributing to their escape from immune surveillance.

To gain more evidence, we performed cell velocity analysis to observe the directions of tumor cell development. We found that most cells from Tumor.C1 were growing in the same direction, moving away from Tumor.C2 (Figure 2G). Combining RNA-seq data from 65 GIST primary and metastasis samples with different AFIP risk classification, we found that most Tumor.C1 cells only mapped into the high and metastasis samples (Figures 2H and S3a), while only Tumor.C2 cells mapped into other lower risk groups (Figure 2H). Such observations strongly agree with our speculation that Tumor.C1 cells were at a late state of tumor progress and could be closely related to metastasis. Another published data set (GSE21315) comprising metastasis and nonmetastasis samples also supports our conclusion (Figure S3b). Together, a path appeared where Tumor.C2 cells grew into Tumor.C1 cells along with tumor progression and metastasis.

To determine what specific genes might be correlated with tumor progress, we performed WGCNA on total tumor cells. Three gene models were identified: MEbrown, MEblue, and MEturquoise (Figure 2I). The MEturquoise gene model (Supporting Information File S1) was the most efficient in distinguishing the two tumor cell types from each other (Figures 2J and S4). We separated the genes in MEturquoise into two groups: Tumor.C1 signature genes and Tumor.C2 signature genes. Based on the signature genes, we calculated the corresponding scores for the 65 sample cohort. Consistent with the results above, Tumor.C1 signature scores were significantly higher in high-risk and metastasis samples compared to the other groups (Figure 2K), while Tumor.C2 signature scores significantly higher in the rest groups (Figure 2L). Another dataset comprising metastasis and nonmetastasis samples was also consistant with our observations (Figure S3c).

On the other hand, although Tumor.C2 appeared relatively "resting" and low risk, it might still promote tumor malignance through up-regulating a series of worse prognostic genes, such as *CD81*,[30] *TIMP1*,[31] *LGALS3BP*,[32] *CD151*,[33] etc, suggesting their "standby" status for transforming into Tumor.C2 cells.

In conclusion, we investigated the heterogeneities of GIST cells, revealed two subgroups of tumor cells for the first time, and found their clinical relevance. Tumor.C1 cells grew quickly, had high DNA damage, and could easily metastasize. They could be enriched in high-risk patients and were associated with worse prognosis.

3.3 | CD8 EM cells were the most expanding but also exhausted cells among all T cells

T cells were hotspot in cancer immunology research recently. However, in GISTs, their heterogeneities and characters have not been well studied. Focusing on T cells, we detected 3443 and 10 323 T cells, accounting for 35.2% and 56.7%, respectively, in patients G1 and G2. We clustered these into 11 subsets (Figures 3A,B and S5) based on cell markers and published immune cell transcriptomes (GSE107011[34]).

Interestingly, we found a great number of $CD8^+$ gamma delta T cells (GDT), which mostly came from patient G2 (Figure 3B). The $CD8^+$ GDT, which showed double positive of alpha and beta domains of CD8

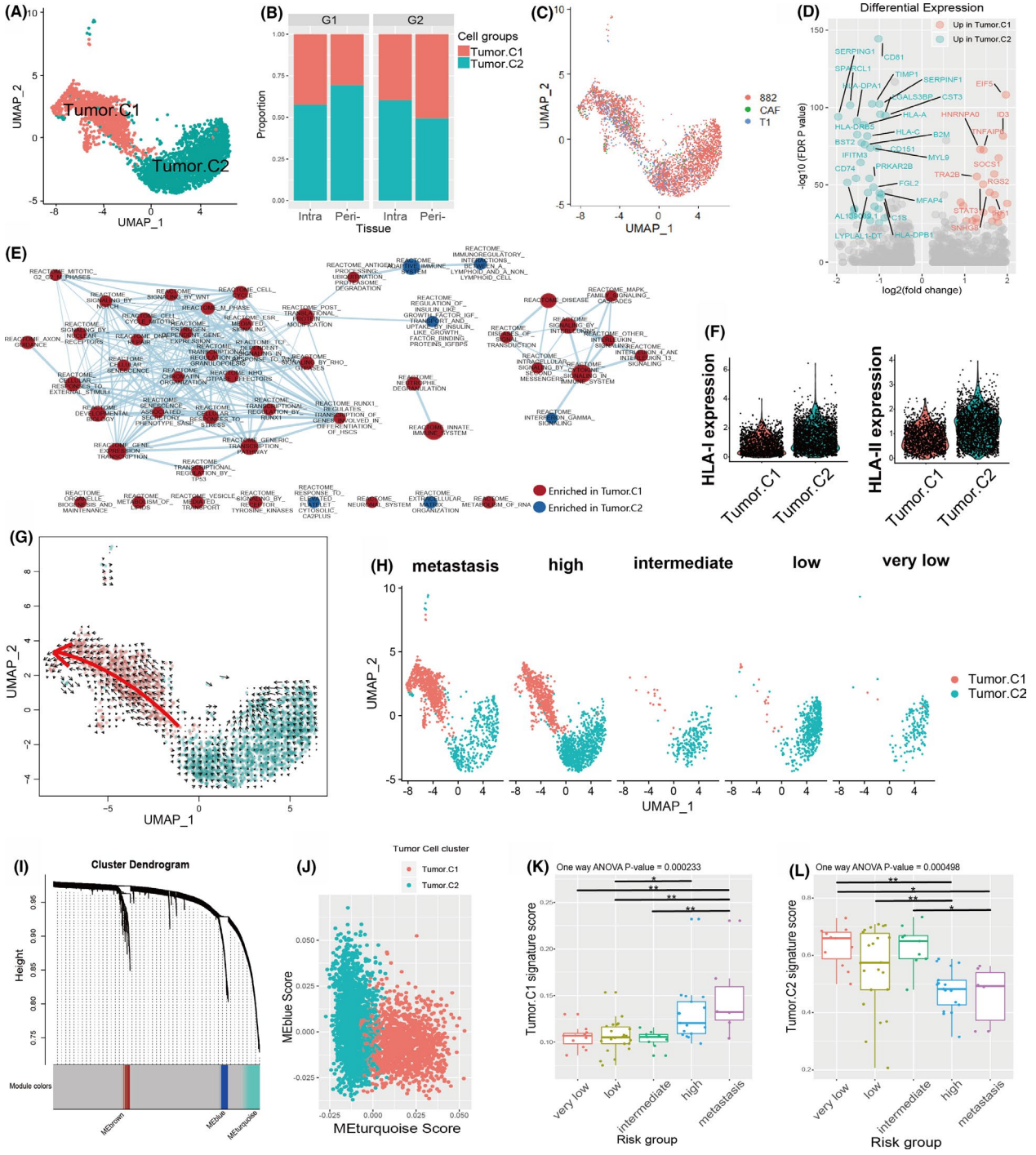

FIGURE 2 Tumor cell heterogeneity. A, UMAP visualization of tumor cells. Two main cell types were observed: Tumor.C1 and Tumor.C2. B, The bar plot of proportions of two tumor cell types in peri- and intra-tissue from patients G1 and G2. C, UMAP visualization of tumor cells labeled by SingleR annotations using GIST cell line (882 and T1) and CAF as reference. D, Volcano plot of gene differential expressions between two tumor cell types: Tumor.C1 and Tumor.C2. E, Networks of pathway enrichment between Tumor.C1 and Tumor.C2. Red circle nodes represent pathways enriched in Tumor.C1, while blue circle nodes represent pathways enriched in Tumor.C2. The size of the circle represents the number of detected pathway genes. The width of the edges represents the number of overlap detected genes between the two pathways. F, Violin plot of HLA expression in Tumor.C1 and Tumor.C2. G, Velocity plot on the UMAP of tumor cells. The red arrow shows the main direction of Tumor.C1 development. H, UMAP visualization of tumor cells separated as cells aligned into different RNA profiles from samples of metastasis and different AFIP risk classifications. I, Hierarchical clustering of high variable genes in tumor cells. Three gene models are identified: MEbrown, MEblue and MEturquoise. J, The scatter plots of gene model scores in tumor cells. K, Boxplot of Tumor.C1 signature scores in 65 GIST RNA-seq samples. Samples are classified by their metastasis status and AFIP classifications. Tumor.C1 and Tumor.C2 signature genes were obtained from the MEturquoise gene model. L, Boxplot of Tumor.C2 signature scores in 65 GIST RNA-seq samples

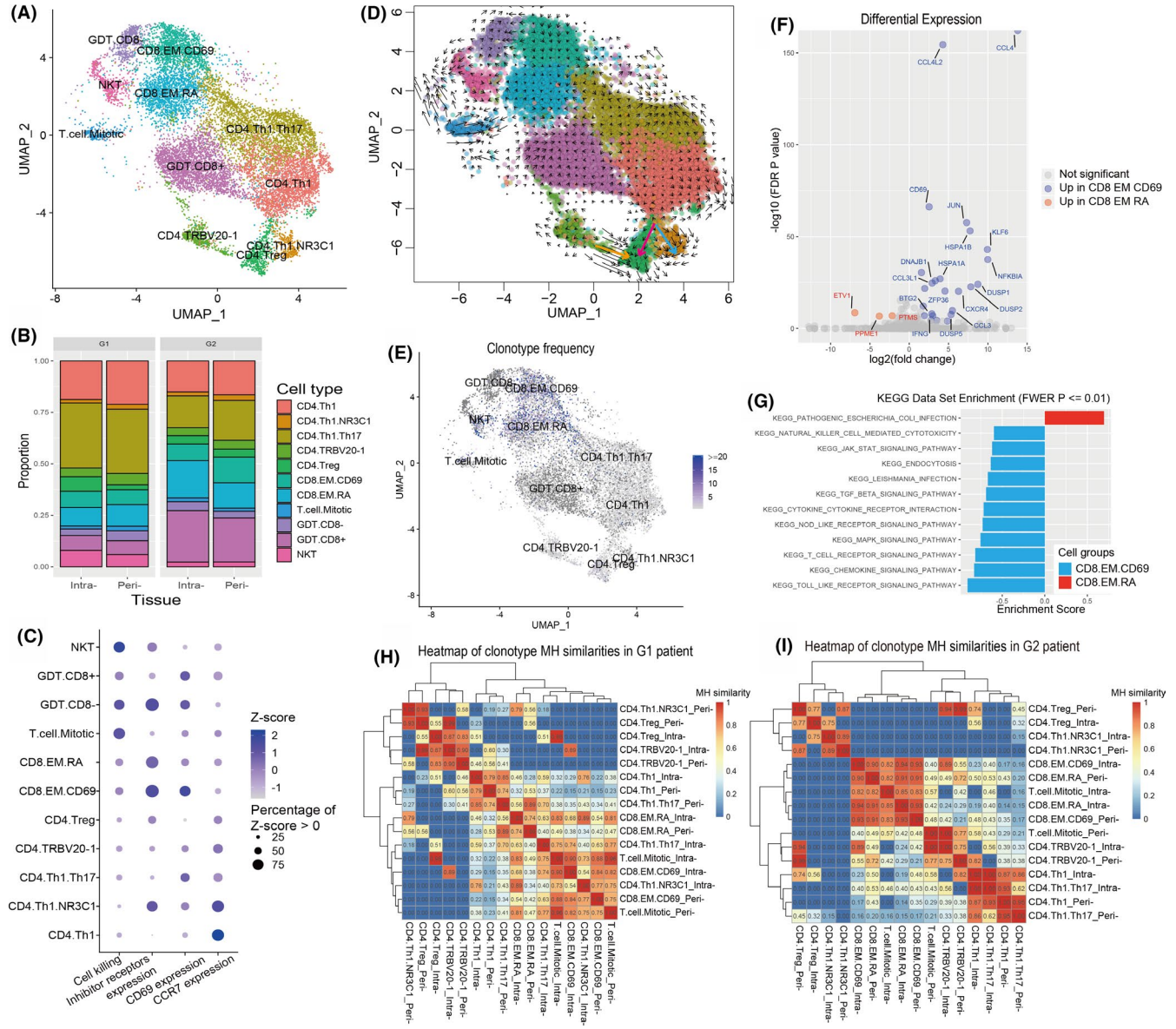

FIGURE 3 Clustering and characterizing T cells. A, UMAP visualization of T cells. T cells belonging to different groups are annotated with different colors. B, Barplot of proportions of T cell subsets in peri- and intra-tissue from patients G1 and G2. C, Dotplot of cell feature scores in all T cell subsets, including scores of cell killing, inhibitor receptor expression, CD69 expression, and CCR7 expression. D, Velocity plot on the UMAP of T cells. Arrows represent the directions of relative T cell development. E, UMAP visualization of clonotype frequencies. For each cell, the color represents the frequency of its clonotype. Cells without TCRs are colored dark grey. F, Volcano plot of differential expressed genes between CD8.EM.CD69 and CD8.EM.RA. I, Barplot of GSEA results from comparing CD8.EM.CD69 and CD8.EM.RA using the gene sets in KEGG. This plot shows the most significant enriched gene sets with a FWER *P* value lower than 0.01. H and I, Heatmaps of clonotype MH similarities among αβ T cell subgroups in both tissues of patients G1 and G2

molecule, was first reported in patients with inflammatory bowel disease as a subset expressing cytotoxic mediators and CD69, enriched in healthy controls and possibly playing an important role in gut homeostasis and mucosal healing.[35] Here in GIST tissues, $CD8^+$ GDT cells also highly expressed CD69 and lowly expressed CCR7 (Figure 3C), showing tissue-resident characters. However, $CD8^+$ GDT showed lower cell killing ability and cell exhaustion than $CD8^-$ GDT. What is more, they overexpressed IFITM1-3 (Figure S6a-c), which was associated with antiviral activities.[36] Therefore, these cells could be related to the personal history of viral infection and were possibly bystanders for GIST.

Here, the majority of CD4 cells were Th1 cells, which were more likely to come from central memory (CM) cells (highly expressed *CCR7*; Figure 3C). Interestingly, there were a group of Th1 cells highly expressed *NR3C1*, a glucocorticoid receptor, which could suppress inflammatory functions. Furthermore, CD4.Th1.NR3C1 cells highly expressed inhibitor receptors (IRs), inferring that this type of cell was extremely exhausted. Based on the velocity analysis (Figure 3D), the CD4.Th1.NR3C1 cells may differentiate from the same linage with Treg cells. The high clonal MH similarities between CD4.Th1.NR3C1 and CD4.Treg (Figure 3H&I) support our speculation. For Tregs, CD4.

TRBV20-1 cells turned into them in fast rates (Figure 3D) and shared high MH similarities (Figure 3H&I), suggesting a continuously supplementary for Tregs.

Notably, both groups of CD8 EM cells were highly exhausted (Figure 3C). The *LAG3* expression contributed most in the exhaustion of these cells (Figure S7), suggesting that anti-LAG-3 therapy may be of most benefit for GIST patients of all the checkpoint blockage therapies. In addition, these two groups were in high clonal expansion (Figure 3G), had intermediate killer cell cytotoxicity and low *CCR7* expression, and had high levels of co-inhibitor receptor expression (Figure 3F). However, expression of *CD69* in CD8.EM.RA was significantly lower than that in CD8.EM.CD69. We also found more genes were significantly up-regulated in CD8.EM.CD69 than in CD8.EM.RA (Figure 3F). The up-regulation of heat shock protein genes, dual-specificity phosphatase genes, and *NKFBIA* referred a higher cell stimulation stress and immune involvement of CD8.EM.CD69. GSEA further showed that CD8.EM.CD69 enriched multiple pathways that participate in inflammatory immune response (Figure 3G). Thus, CD8.EM.CD69 was more involved in immune response in the tumor microenvironment, while the CD8.EM.RA cells appeared to be lower-functionalized, recently activated bystander T cells.

It has been reported that GISTs with high densities of $CD3^+$ cells had better outcomes.[37] However, the correlation between tumor-infiltrating T cells and risk classifications is still ambiguous. In bulk RNA-seq data, we found that T cell enrichment scores were significantly higher in the metastasis site (Figure S8A), consisted with a previous report,[38] but $CD8^+$ cells and $CD4^+$ cells did not show a significant difference between primary and metastasis sites (Figure S8B,C) What is more, in general we did not observed significant correlations between T cell enrichments and AFIP risks.

In conclusion, we found that in GIST, the pro-inflammation and cell killing ability of T cells was suppressed. Cells with high cytotoxicity were mostly exhausted, or with very limited cell number as natural killer T cells (NKTs). Cells with potential cytotoxicity, such as GDT.CD8+ and CD8.EM.RA, were likely to act as recently activated or bystanders. In addition, Tregs were continuously supplemented by other cell groups, thus enhancing anti-inflammation. This observation might help us in developing T-cell immunotherapies for GISTs.

3.4 | A group of macrophages exhibit both anti- and pro-inflammatory functions

Monocytes are a class of cells with high heterogeneities. Macrophages were found to be correlated with prognosis in multiple cancers.[39,40] However, how macrophages polarized in GIST is still unknown. MMDs were one of the major cell types we found in GIST tissues. We observed 1828 and 3258 effective MMDs, accounting for 18.7% and 17.9% of total cells, respectively, in patients G1 and G2. As shown in Figure S9, MMDs highly and specifically expressed *C1QA/B/C*, *AIF1*, *CD68*, *MS4A6A*, etc.

To invest MMD heterogeneity, we classified them into eight groups (Figure 4A). We found that the largest group of MMDs enriched both M1 and M2 characters (Figure 4B,C), suggesting that this group may perform both pro- and anti-inflammatory functions. Next we compared our MMDs to the cell line data (GSE135165[24]) of monocyte THP-1 and macrophages differentiated from THP-1 to calculate the macrophage polarized scores (Figure 4D). We found that Mac.C1.FOS.CCL3 and Mac.C6.MT2A were the most polarized, while Mac.C2, dendritic cell (DC), and monocytes the least. We obtained similar results (Figure S10a,b) by comparing our macrophages to monocytes and TAMs in endometrial and breast cancers (GSE117970[25]), suggesting that these highly polarized groups might be TAM-like macrophages.

By investigating the correlations between each MMD group, Mac.C2, DC, and Monocytes were found to be clustered (Figure 4E), confirming that the Mac.C2 cells were at the very beginning of macrophage polarization, which was also supported by the analysis above (Figures 4D and S10A,B). Next, we used a diffusion map[17] to construct a cell developmental pseudo-time trajectory and observed a major path of macrophage polarization along the DM1 axis (Figure 4F) starting at Mac.C2 and ending in Mac.C1.FOS.CCL3. The cell group of Mac.C3.CXCL9.10.11, Mac.C4.IFI27, and Mac.C5.APOE could be observed along the axes of DM3, DM4, and DM2, respectively. All these cell groups had intermediate values of DM1 and could be followed from both the starting and ending of polarization, suggesting that subgroups of macrophage were able to transform to each other, no matter in which state of the polarization, supporting the conclusion that macrophages have the potential to modify their functions under the influence of specific signals.[41] Interestingly,

FIGURE 4 Cell heterogeneities of macrophages reveal the path of their polarization. A, UMAP visualization of macrophage heterogeneities. Eight groups of MMDs are shown. B, Barplot of the M1 signature scores of MMD cells grouped by the eight cell groups. M1 signature scores were calculated based on the pro-inflammation-related genes of macrophages, including IL1B, TNF, IL12A, IL18, CD68, CD80, CD86, SOCS3, IRF5, STAT1, and RELA. C, Barplot of the M2 signature scores of MMD cells grouped by the eight cell groups. M2 signature scores were calculated based on the anti-inflammation-related genes of macrophages, including MRC1, IL10, CD200R1, CD163, LLGL1, LLGL2, RGCC, STAT6, STAT3, NFKB1, and IRF4. "AUCell" was used for the M1 and M2 score calculations. D, UMAP visualization of macrophage polarization scores of all MMDs. The macrophage polarization scores were calculated based on the published data (GSE135165), in which the transcriptomes of monocytes THP-1 and macrophages differentiated from monocytes THP-1 were collected. E, Heatmap of MMD cell group correlation. Cell group correlation values were calculated between gene expressions of each two cell groups. These values were used to estimate the similarities among all groups. F, Diffusion map visualization of macrophage polarization. G, Volcano plot of gene differential expression between Mac.C1.FOS.CCL3 and Mac.C2. H, Violin plot of HLA molecule expression in Mac.C1.FOS.CCL3 and Mac.C2. I, Barplot of macrophage polarization scores in the bulk RNA-seq cohort. Macrophage polarization scores were calculated using the top 30 significantly marker genes up-regulated in Macrophage.C1.CCL3 compared to Macrophage.C2

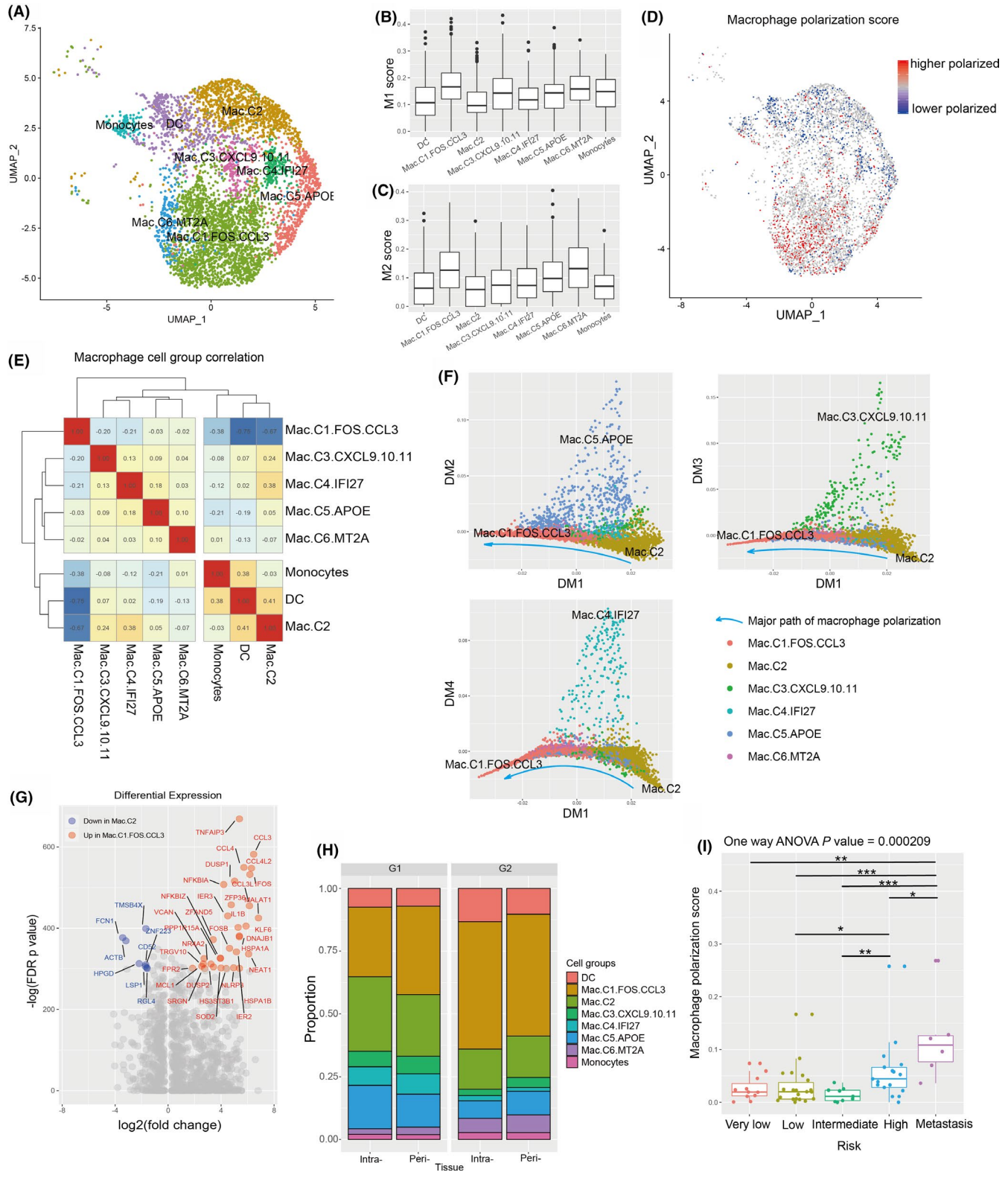

we found that Mac.C3.CXCL9.10.11 highly expresses CXCL9 and CXCL10, which could recruit NK and CD8$^+$ T cells and inhibited angiogenesis[42] showing pure anti-tumor activities. However, the cell volume of this group was very low in GIST tissues.

The major path of macrophage polarization shows how macrophages are polarized in GISTs. By comparing Mac.C2 and Mac.C1.FOS.CCL3 (Figure 4G), we found that genes involved in the NF-kappa-B pathway and the AP-1 transcription factor family, such as *IL1B*, *NFKBIA*, and *TNFAIP3*, as well as *FOS* and *FOSB*, were up-regulated in highly polarized Mac.C1.FOS.CCL3. Notably, these macrophages also highly expressed CCL3 and CCL4. CCL4 in collaboration with CCL3 has diverse effects on immune and nonimmune cells such

as macrophages, Tregs, fibroblasts, and endothelial cells to facilitate their pro-tumorigenic capacity.[43,44] In addition, this group of macrophages expressed lower HLA molecules, especially HLA-II, compared to the less polarized macrophages (Mac.C2) (Figure S10C). Such observations suggest that the antigen-presenting function declined accompanied by macrophage polarization in GIST, which might also contribute to tumor growth. Consistently, the polarized macrophages (Mac.C1) accounted for a higher proportion in high-risk patient G2 (Figure 4H and S10D). More importantly, in the bulk RNA-seq cohort, macrophage polarization increased along with tumor malignancy (Figure 4I), supporting our conclusion and indicating their prognostic values.

In general, we revealed heterogeneities of MMDs and discovered how macrophages polarize in GISTs, which has not been well described in previous reports. The highly polarized macrophages possess functions of both anti- and pro-inflammations, might contribute to tumor malignancy, and have prognostic values. Such observations highlight the importance of macrophage polarizations in GIST microenvironments.

3.5 | Heterogeneity of NK cells in GIST

NK cells also exhibit heterogeneity in GIST. We classified NK cells into four different cell groups (Figure S11A,B) and noticed that NK.C3. Mitotic was at the mitosis state of the cell cycle and correlated with the diffusion map component 1 (DM1) (Figure S11c). Combining the pseudo-time trajectory with cell velocity, we found a cell differentiation path from NK.C0 cells to NK.C2.GNLY cells (red arrow in Figure S11D), and finally to NK.C1.CD69 cells. To describe this path, we first investigated the NK.C0 cells. We found that they were very stable and did not have significantly up-regulated gene markers compared to the other NK cell groups (Figure S11B). Then, by comparing NK.C1.CD69 and NK.C2.GNLY, we found that NK.C1.CD69 cells highly expressed genes in NF-kappa-B pathway and AP-1 family (Figure S11e), such as *NFKBIA*, *TNFAIP3* and *JUNB CCL3* and *CCL4* were also up-regulated in NK.C1.CD69. Pathways enriched in NK.C1.CD69 were more cancer-related (Figure S11f). Since they also highly expressed *CD69*, we might infer that this group was likely to be tumor-reactive, and the path from NK.C2.GNLY to NK.C1.CD69 reflected an NK activation trajectory. What is more, we also noticed that most NK.C2.GNLY cells were in fast transition rates, suggesting their intermediate state in NK cell activation. In conclusion, we found a cell differentiation path from the original NK.C0 cells to the intermediate NK.C2.GNLY cells, and finally to the activated NK.C1.CD69 cells.

3.6 | Cell-to-cell interactions revealed adipose endothelial cells had high interactions with tumor cells to facilitate tumor growth

Cell interactions are key factors for tumor development. Based on cell surface protein interactions, we traced interactions among all cells in both patients to provide a full view of the tumor microenvironment. As shown in Figures 5A and S12A, two tumor groups had high interactions with each other and with adipose endothelial cells. As expected, collagen proteins tightly connected GISTs and adipose endothelial cells spatially (Figure 5B). CD74 were found to be highly involved in such interactions by binding secreted proteins and cell surface receptors, such as MIF, APP, and COPA (Figure 5B), thus are likely to playing an important role in promoting tumor progression, according to previous research.[45-48]

Additionally, we found some interactions uniquely from adipose endothelial cells (Figure 5B, in the red boxes) that might affect tumor growth. First, adipose endothelial cells expressed LAGLS9 and PDGFB binding to LRP1, which can enhance expression of collagen 1,[49] thus consolidating the connection between tumor cells and adipose endothelial cells. Second, adipose endothelial cells expressed EFNA1 binding with EPHA7 and EPHA4, both of which were reported to accelerate tumor growth.[50-52] In return, tumor cells expressed DLK1 binding with Notch4 (Figure 5B, in blue box) to positively regulate proliferation of adipose endothelial cells. Therefore, a vicious circle was established facilitating tumor malignancy. Breaking this circle by targeting key molecules could be beneficial to GIST patients.

To confirm that interactions from adipose endothelial cells might promote tumor malignances, we again made use of bulk RNA-seq samples. Based on the top 30 gene markers that uniquely expressed in adipose endothelial cells, we found that adipose endothelial cells were significantly high in metastasis (Figure 5C), supporting the finding that these cells might have a large impact on facilitating tumor metastasis.

3.7 | Macrophages were found to have strong recruiting ability at the center of the cell interaction network

We investigated cell chemokine interactions among all cell types in both patients (Figures 5D and S12B). These chemokine interactions revealed immune cells trafficking and loops that total cells were involved. In total, we found 74 chemokine interactions forming three major interaction clusters (Figure 5D). Macrophages participates all major clusters. Consisted with our previous results, Mac.C3.CXCL9.10.11 was found to perform as an antitumor factor to express most chemokine and strongly recruiting Th1, CD8 cells, NKTs and GDT cells, which are widely believed to correlate with better prognosis in multiple types of cancers.

In general, macrophages displayed at the center niche of the cell interaction network, connected all cell types in the tumor microenvironment, and played an important role in maintaining immune homeostasis. In addition, the bulk RNA-seq cohort showed that macrophages were reduced in the primary site of patients with higher AFIP risks (Figure 5E), consistent with the finding that tumor progression is strongly associated with the collapse of immune homeostasis in the primary site of tumor genesis.

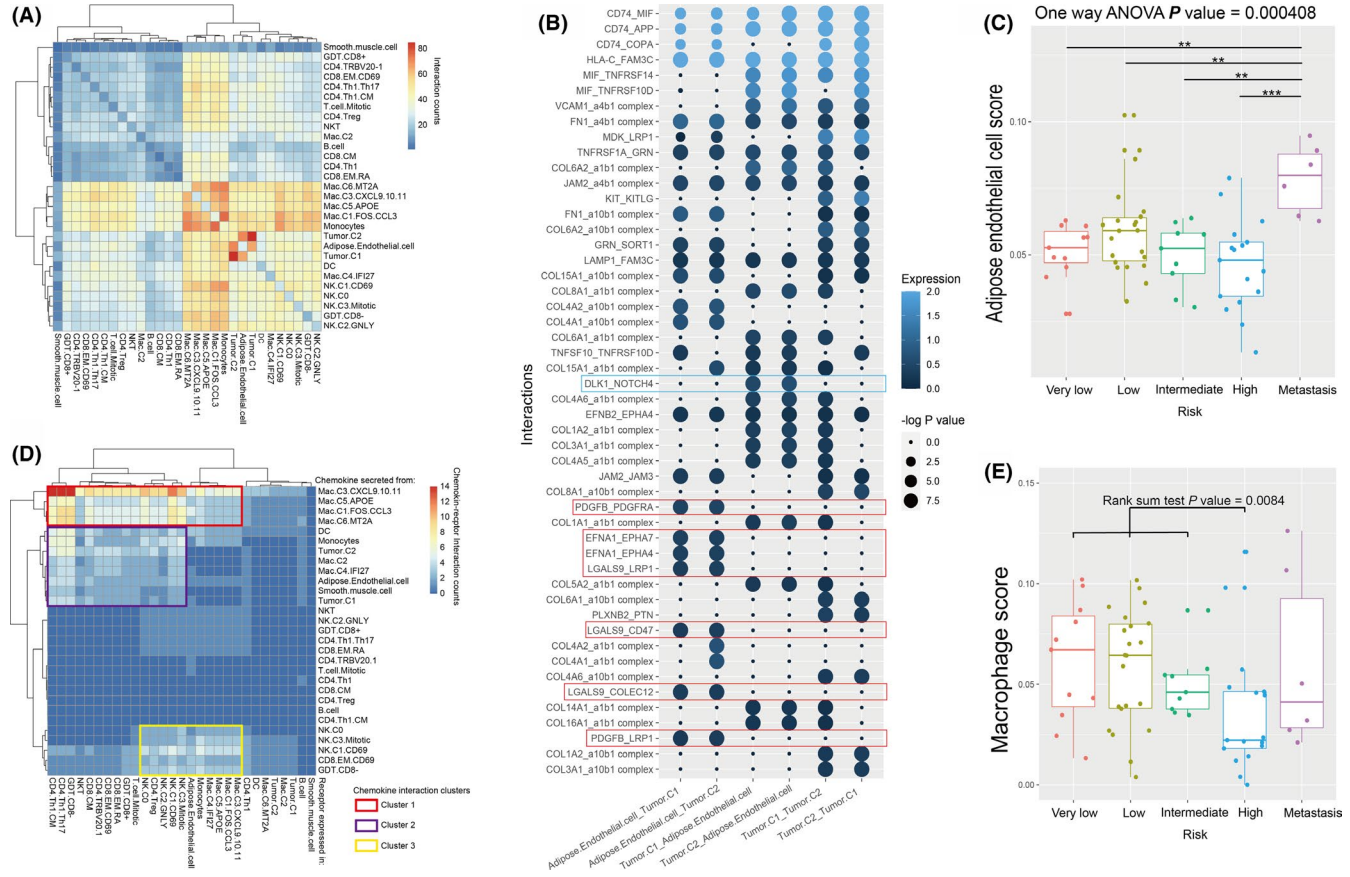

FIGURE 5 Cell interaction networks. A, Heatmap of cell group interaction counts. B, Dotplot of molecule interactions between tumor cells and adipose endothelial cells. The red boxes show interactions uniquely from adipose endothelial cells to tumor cells. The blue box shows a feedback interaction from tumor cells to adipose endothelial cells. C, Boxplot of adipose endothelial cell enrichment scores of 65 GIST bulk RNA-seq samples. Scores were calculated using the top 30 marker genes for adipose endothelial cells. D, Heatmap of chemokine interaction among cell groups. Chemokins were secreted from the cell groups in rows, and the corresponding receptors were expressed in cell groups in columns. The three major chemokine interaction clusters are shown in red, purple, and yellow boxes. E, Boxplot of macrophage enrichment scores of 65 GIST bulk RNA-seq samples. Scores were calculated using the top 30 marker genes for macrophages

4 | DISCUSSION

We performed single-cell sequencing of peri- and intra-tumor tissue from two GIST patients with low and high risk. Although abundances of some cell types were limited, the predominated cell types were adequate to conduct downstream analysis.

By investigating tumor cell heterogeneity, we observed two groups of tumor cells separated by their proliferation rates. Signatures from cells with fast proliferation were associated with a high risk of tumor malignancy and metastasis, which was confirmed in a cohort of 65 GISTs in Japan, referring such signatures could be used as prognosis indicators or as supplements for AFIP classification. This is the first time AFIP risks have been associated with tumor cells at the single-cell transcriptome level, and this also provides evidence for cancer prognosis and therapy. Interaction analysis also showed that two tumor groups are in high interactions with each other and had tight connection with the adipose endothelial cells. Adipose tissue cell populations were reported to influence the development of cancer cells and increase the risk of metastasis as well as shorten patient survival.[53] Apart from CD74, some molecules were found to play very important roles in tumor-adipose interactions. Targeting these molecules might help to inhibit tumor growth, providing a new strategy in cancer therapy.

In this research, we did not find a great difference in fast proliferating tumor cells between the high- (G2) and low-risk (G1) patients in our research. This may be caused by imatinib therapy before surgery for the high-risk patient G2, while no therapy was applied in the low-risk patient G1 before surgery. The imatinib therapy had great efficacy in treating GIST as for patient G2. Tumor size shrank after the therapy, and the mitosis count was at a low level, suggesting that the fast proliferating cells were under control.

We observed a high proportion of T cells in the tumor tissue of patient G2. In addition, B cells were highly enriched in patient G2 (Figure S1), although the total number of B cells was very low. These results indicate that imatinib therapy might enhance tumor lymphocyte infiltration. Such speculation is also supported by recent research studying relations among immune infiltration, imatinib response, and patient survival.[54] Among all T cells found in GISTs, only CD8 EM cells were in high expansion. Furthermore, CD8 EM cells highly expanded and shared clonal types in both intra- and peri-tumor tissues, suggesting common antigens might exist. However,

further experiments are needed to demonstrate whether these CD8 EM cells are tumor reactive or just bystanders, according to a published research.[55] For CD8 cells in GIST, it has been reported that these cells could be rescued by PD-1/PD-L1 therapy.[56] Indeed, CD8 cells were the most exhausted T cells in GIST tissue. However, they were not the most PD-1 expressing cells. Instead, CD4 Th1 cells express the highest PD-1. Among the five co-inhibitor genes we investigated (Figure S7), CD8 cells highly expressed LAG-3, indicating that targeting the LAG-3 could be beneficial.

Macrophages were at the center of the tumor microenvironment, helping to build connections between tumor cells and other cell types, and were also most affected by signals from other cells forming specific polarized statuses. Typically, the polarizations of macrophage were described as pro-inflammatory (M1) and anti-inflammatory (M2) polarizations. TAMs were once thought to perform M2-like functions and lead to tumor growth and metastasis.[57] In GISTs, we found that TAM-like macrophages simultaneously had both M1 and M2 signatures, which were also supported by other single-cell research in breast cancer[58] and hepatocellular carcinoma.[59] However, there are still controversies surrounding the roles that TAMs play in the tumor microenvironment.[60] Interestingly, we found polarized macrophages increased but total macrophages decreased accompanied by tumor progression in GIST, emphasizing the role of macrophages in the tumor microenvironment.

In this study, B cells did not seem to be highly involved and displayed low abundance in the GIST. In fact, recent evidence has proved that B cells participate in the tumor microenvironment and help to activate T cells and create an immunotherapy response, which has a very important role in prolonging the survival of patients treated with checkpoint blockages.[61,62] The absence of B cells in GIST might contribute to tumor growth, which is also worthy of investigation in future studies.

In this study, we obtained an overview of the GIST microenvironment and revealed the heterogeneity of each cell type and their relevance to AFIP risk classifications, which provides a novel theoretical basis for learning and curing GISTs.

ACKNOWLEDGMENT

This work was funded by grants from the National Natural Science Foundation of China (81972335), the Foundation and Applied Basic Research Fund of Guangdong Province (2019A1515110677, 2019A1515110676), the Science and Technology Innovation Platform in Foshan City (FS0AA-KJ218-1301-0007) and the Foshan city climbing peak plan (2019A004, 2019D036, 2019D035), Medical Engineering Technology Research and Development Center of Immune Repertoire in Foshan.

DISCLOSURE

The authors declare no potential conflict of interest.

ORCID

Wei Luo https://orcid.org/0000-0002-8836-3804

REFERENCES

1. Judson I, Demetri G. Advances in the treatment of gastrointestinal stromal tumours. *Ann Oncol*. 2007;18(Suppl 10):x20-x24.
2. Nishida T, et al. The standard diagnosis, treatment, and follow-up of gastrointestinal stromal tumors based on guidelines. *Gastric Cancer*. 2016;19(1):3-14.
3. El-Menyar A, Mekkodathil A, Al-Thani H. Diagnosis and management of gastrointestinal stromal tumors: an up-to-date literature review. *J Cancer Res Ther*. 2017;13(6):889-900.
4. Joensuu H, Hohenberger P, Corless CL. Gastrointestinal stromal tumour. *Lancet*. 2013;382(9896):973-983.
5. Schaefer IM, Marino-Enriquez A, Fletcher JA. What is new in gastrointestinal stromal tumor? *Adv Anat Pathol*. 2017;24(5):259-267.
6. Sanders KM, Ward SM, Koh SD. Interstitial cells: regulators of smooth muscle function. *Physiol Rev*. 2014;94(3):859-907.
7. Akahoshi K, Oya M, Koga T, Shiratsuchi Y. Current clinical management of gastrointestinal stromal tumor. *World J Gastroenterol*. 2018;24(26):2806-2817.
8. Hirota S. Differential diagnosis of gastrointestinal stromal tumor by histopathology and immunohistochemistry. *Transl Gastroenterol Hepatol*. 2018;3:27.
9. Fletcher CD, Berman JJ, Corless C, et al. Diagnosis of gastrointestinal stromal tumors: a consensus approach. *Int J Surg Pathol*. 2002;10(2):81-89.
10. Miettinen M, Lasota J. Gastrointestinal stromal tumors: pathology and prognosis at different sites. *Semin Diagn Pathol*. 2006;23(2):70-83.
11. Demetri GD, Benjamin RS, Blanke CD, et al. NCCN Task Force report: management of patients with gastrointestinal stromal tumor (GIST)–update of the NCCN clinical practice guidelines. *J Natl Compr Canc Netw*. 2007;5(Suppl 2):S1-29; quiz S30.
12. Hafemeister C, Satija R. Normalization and variance stabilization of single-cell RNA-seq data using regularized negative binomial regression. *Genome Biol*. 2019;20(1):296.
13. Stuart T, et al. Comprehensive integration of single-cell data. *Cell*. 2019;177(7):1888-1902 e21.
14. Martens JH, Stunnenberg HG. BLUEPRINT: mapping human blood cell epigenomes. *Haematologica*. 2013;98(10):1487-1489.
15. The ENCODE Project Consortium. An integrated encyclopedia of DNA elements in the human genome. *Nature*. 2012;489(7414):57-74.
16. Aran D, Looney AP, Liu L, et al. Reference-based analysis of lung single-cell sequencing reveals a transitional profibrotic macrophage. *Nat Immunol*. 2019;20(2):163-172.
17. Haghverdi L, Büttner M, Wolf FA, Buettner F, Theis FJ. Diffusion pseudotime robustly reconstructs lineage branching. *Nat Methods*. 2016;13(10):845-848.
18. La Manno G, et al. RNA velocity of single cells. *Nature*. 2018;560(7719):494-498.
19. Subramanian A, et al. Gene set enrichment analysis: a knowledge-based approach for interpreting genome-wide expression profiles. *Proc Natl Acad Sci USA*. 2005;102(43):15545-15550.
20. Jassal B, et al. The reactome pathway knowledgebase. *Nucleic Acids Res*. 2020;48(D1):D498-D503.
21. Kanehisa M, Furumichi M, Tanabe M, Sato Y, Morishima K. KEGG: new perspectives on genomes, pathways, diseases and drugs. *Nucleic Acids Res*. 2017;45(D1):D353-D361.
22. Godec J, Tan Y, Liberzon A, et al. Compendium of immune signatures identifies conserved and species-specific biology in response to inflammation. *Immunity*. 2016;44(1):194-206.
23. Shannon P. Cytoscape: a software environment for integrated models of biomolecular interaction networks. *Genome Res*. 2003;13(11):2498-2504.
24. Diaz-Jimenez D, Petrillo MG, Busada JT, Hermoso MA, Cidlowski JA. Glucocorticoids mobilize macrophages by transcriptionally up-regulating the exopeptidase DPP4. *J Biol Chem*. 2020;295(10):3213-3227.

25. Cassetta L, Fragkogianni S, Sims AH. Human tumor-associated macrophage and monocyte transcriptional landscapes reveal cancer-specific reprogramming, biomarkers, and therapeutic targets. *Cancer Cell*. 2019;35(4):588-602 e10.
26. Zhang B, Horvath S. A general framework for weighted gene co-expression network analysis. *Stat Appl Genet Mol Biol*. 2005;4:p. Article17.
27. Hindley JP, Ferreira C, Jones E, et al. Analysis of the T-cell receptor repertoires of tumor-infiltrating conventional and regulatory T cells reveals no evidence for conversion in carcinogen-induced tumors. *Cancer Res*. 2011;71(3):736-746.
28. Efremova M, Vento-Tormo M, Teichmann SA, Vento-Tormo R. Cell PhoneDB: inferring cell-cell communication from combined expression of multi-subunit ligand-receptor complexes. *Nat Protoc*. 2020;15(4):1484-1506.
29. Ohshima K, Fujiya K, Nagashima T, et al. Driver gene alterations and activated signaling pathways toward malignant progression of gastrointestinal stromal tumors. *Cancer Sci*. 2019;110(12):3821-3833.
30. Mizoshiri N, Shirai T, Terauchi R, et al. The tetraspanin CD81 mediates the growth and metastases of human osteosarcoma. *Cell Oncol (Dordr)*. 2019;42(6):861-871.
31. Grunwald B, Schoeps B, Kruger A. Recognizing the molecular multifunctionality and interactome of TIMP-1. *Trends Cell Biol*. 2019;29(1):6-19.
32. Marchetti A, Tinari N, Buttitta F, et al. Expression of 90K (Mac-2 BP) correlates with distant metastasis and predicts survival in stage I non-small cell lung cancer patients. *Cancer Res*. 2002;62(9):2535-2539.
33. Sadej R, Grudowska A, Turczyk L, Kordek R, Romanska HM. CD151 in cancer progression and metastasis: a complex scenario. *Lab Invest*. 2014;94(1):41-51.
34. Xu W, Monaco G, Wong EH, et al. Mapping of gamma/delta T cells reveals Vdelta2+ T cells resistance to senescence. *EBioMedicine*. 2019;39:44-58.
35. Kadivar M, Petersson J, Svensson L, Marsal J. CD8alphabeta+ gammadelta T cells: a novel T cell subset with a potential role in inflammatory bowel disease. *J Immunol*. 2016;197(12):4584-4592.
36. Bailey CC, Zhong G, Huang I-C, Farzan M. IFITM-family proteins: the cell's first line of antiviral defense. *Annu Rev Virol*. 2014;1:261-283.
37. Rusakiewicz S, Semeraro M, Sarabi M, et al. Immune infiltrates are prognostic factors in localized gastrointestinal stromal tumors. *Cancer Res*. 2013;73(12):3499-3510.
38. Cameron S, Gieselmann M, Blaschke M, Ramadori G, Füzesi L. Immune cells in primary and metastatic gastrointestinal stromal tumors (GIST). *Int J Clin Exp Pathol*. 2014;7(7):3563-3579.
39. Chen Z, Feng Xi, Herting CJ, et al. Cellular and molecular identity of tumor-associated macrophages in glioblastoma. *Cancer Res*. 2017;77(9):2266-2278.
40. Xue Y, Tong L, Liu F, et al. Tumor infiltrating M2 macrophages driven by specific genomic alterations are associated with prognosis in bladder cancer. *Oncol Rep*. 2019;42(2):581-594.
41. Juhas U, Ryba-Stanisławowska M, Szargiej P, Myśliwska J. Different pathways of macrophage activation and polarization. *Postepy Hig Med Dosw* (Online). 2015;69:496-502.
42. Nagarsheth N, Wicha MS, Zou W. Chemokines in the cancer microenvironment and their relevance in cancer immunotherapy. *Nat Rev Immunol*. 2017;17(9):559-572.
43. Ntanasis-Stathopoulos I, Fotiou D, Terpos E. CCL3 signaling in the tumor microenvironment. *Adv Exp Med Biol*. 2020;1231:13-21.
44. Mukaida N, Sasaki SI, Baba T. CCL4 Signaling in the tumor microenvironment. *Adv Exp Med Biol*. 2020;1231:23-32.
45. De R, Sarkar S, Mazumder S, et al. Macrophage migration inhibitory factor regulates mitochondrial dynamics and cell growth of human cancer cell lines through CD74-NF-kappaB signaling. *J Biol Chem*. 2018;293(51):19740-19760.
46. Imaoka M, Tanese K, Masugi Y, Hayashi M, Sakamoto M. Macrophage migration inhibitory factor-CD74 interaction regulates the expression of programmed cell death ligand 1 in melanoma cells. *Cancer Sci*. 2019;110(7):2273-2283.
47. Wu X, Chen S, Lu C. Amyloid precursor protein promotes the migration and invasion of breast cancer cells by regulating the MAPK signaling pathway. *Int J Mol Med*. 2020;45(1):162-174.
48. Xu J, Ying Y, Xiong G, Lai L, Wang Q, Yang Y. Amyloid beta precursor protein silencing attenuates epithelial mesenchymal transition of nasopharyngeal carcinoma cells via inhibition of the MAPK pathway. *Mol Med Rep*. 2019;20(1):409-416.
49. Zucker MM, Wujak L, Gungl A, et al. LRP1 promotes synthetic phenotype of pulmonary artery smooth muscle cells in pulmonary hypertension. *Biochim Biophys Acta Mol Basis Dis*. 2019;1865(6):1604-1616.
50. Li R, Sun Y, Jiang A, et al. Knockdown of ephrin receptor A7 suppresses the proliferation and metastasis of A549 human lung cancer cells. *Mol Med Rep*. 2016;13(4):3190-3196.
51. Hachim IY, Villatoro M, Canaff L, et al. Transforming growth factor-beta regulation of ephrin type-A receptor 4 signaling in breast cancer cellular migration. *Sci Rep*. 2017;7(1):14976.
52. Dong Y, Liu Y, Jiang A, Li R, Yin M, Wang Y. MicroRNA-335 suppresses the proliferation, migration, and invasion of breast cancer cells by targeting EphA4. *Mol Cell Biochem*. 2018;439(1–2):95-104.
53. Cozzo AJ, Fuller AM, Makowski L. Contribution of adipose tissue to development of cancer. *Compr Physiol*. 2017;8(1):237-282.
54. Wei ZW, Wu J, Huang W-B, et al. Immune-infiltration based signature as a novel prognostic biomarker in gastrointestinal stromal tumour. *EBioMedicine*. 2020;57:102850.
55. Scheper W, Kelderman S, Fanchi LF, et al. Low and variable tumor reactivity of the intratumoral TCR repertoire in human cancers. *Nat Med*. 2019;25(1):89-94.
56. Zhao R, Song Y, Wang Y, et al. PD-1/PD-L1 blockade rescue exhausted CD8+ T cells in gastrointestinal stromal tumours via the PI3K/Akt/mTOR signalling pathway. *Cell Prolif*. 2019;52(3):e12571.
57. Josephs DH, Bax HJ, Karagiannis SN. Tumour-associated macrophage polarisation and re-education with immunotherapy. *Front Biosci (Elite Ed)*. 2015;7:293-308.
58. Azizi E, Carr AJ, Plitas G, et al. Single-cell map of diverse immune phenotypes in the breast tumor microenvironment. *Cell*. 2018;174(5):1293-1308 e36.
59. Zhang Q, He Y, Luo N, et al. Landscape and dynamics of single immune cells in hepatocellular carcinoma. *Cell*. 2019;179(4):829-845 e20.
60. Tamura R, Tanaka T, Yamamoto Y, Akasaki Y, Sasaki H. Dual role of macrophage in tumor immunity. *Immunotherapy*. 2018;10(10):899-909.
61. Hollern DP, Xu N, Thennavan A, et al. B cells and T follicular helper cells mediate response to checkpoint inhibitors in high mutation burden mouse models of breast cancer. *Cell*. 2019;179(5):1191-1206 e21.
62. Cabrita R, Lauss M, Sanna A, et al. Tertiary lymphoid structures improve immunotherapy and survival in melanoma. *Nature*. 2020;577(7791):561-565.

SUPPORTING INFORMATION

Additional supporting information may be found online in the Supporting Information section.

How to cite this article: Mao X, Yang X, Chen X, et al. Single-cell transcriptome analysis revealed the heterogeneity and microenvironment of gastrointestinal stromal tumors. *Cancer Sci*. 2021;112:1262–1274. https://doi.org/10.1111/cas.14795